DIAGNOSING DIAPYCNAL MIXING

Kraig B. Winters and Eric A. D'Asaro

Applied Physics Laboratory
Departments of Applied Mathematics and Oceanography
University of Washington, Seattle, WA 98105

ABSTRACT

The diapycnal mixing associated with a small scale mixing event is discussed. A direct numerical simulation of a wave packet propagating through a density stratified shear flow and breaking at a critical level is used to illustrate the issues involved in diagnosing mixing. An indirect approach, based on the density variance equation, is shown to be an ambiguous indicator of mixing. A direct approach, based on the simple idea that net mixing implies a change in the volume of fluid enclosed by a given pair of isopycnals is presented, along with a potential energy analysis and an estimate of the mixing efficiency of the event.

INTRODUCTION

The role of diapycnal mixing in maintaining the large scale heat balance is an important unresolved issue in small scale oceanography. Although the relative contributions to the overall mixing from the interior and at boundaries is in question, much of the diapycnal mixing in the ocean interior is thought to result from isolated, intermittent turbulent "events". Quantifying the mixing associated with a given event is not an easy task. Observational efforts have attempted to determine the diapycnal diffusivity of mass K_d. Generally, measurements of the dissipation rates of kinetic energy or temperature variance are used to infer net vertical fluxes or diffusivity, based on assumed dynamical balances. A review of these techniques can be found in Gregg (1987) or in Moum (1989). The validity of the assumed balances, however, has not yet been well established for the variety of dynamical mechanisms capable of producing turbulent mixing events. From a theoretical viewpoint, it is not clear what type of sampling and averaging is necessary to separate the reversible small-scale internal wave fluxes from the turbulent fluxes.

Large scale ocean circulation models depend critically on details of the parameterization of small scale mixing. Understanding the diapycnal mixing of individual events is an important early step toward the eventual parameterization of small-scale processes and predicting their effects on the large-scale ocean circulation. In this paper, we will focus on the issue of diagnosing the diapycnal mixing of an isolated turbulent mixing event. A high resolution, three-dimensional primitive equation model will be used to generate a mixing event, similar to what may be seen in the ocean

interior. The simulation is similar in spirit to the two-dimensional calculation of Winters and D'Asaro (1989). In the simulated flow, a spatially isolated internal wave packet propagates vertically into a horizontal shear flow. The wave packet is refracted by the background shear, ultimately reaching a critical level where the horizontal phase speed matches the ambient flow speed. Near the critical level, the wave becomes highly nonlinear, developing localized overturns and high shears. The wave breaks through a three-dimensional instability and energy is driven to small scales, where it is rapidly lost to dissipation and diffusion. The instability mechanism is discussed in Winters and Riley (1991). Our interest here is in the diffusive mixing associated with the event.

We will first attempt to diagnose the mixing indirectly, by appealing to the density (or temperature) variance equation. This approach is shown to be problematic, as the production of density variance can be accomplished both by adiabatic (nonmixing) as well as diabatic (mixing) effects. We then illustrate a direct method in which the two effects are isolated. The method is conceptually simple, based on the idea that mixing implies changing the volume of fluid between given isopycnals. This idea leads naturally to the concepts of available and background potential energy which are also useful for diagnosing diffusive mixing.

FLOW SIMULATION

A mixing event is simulated by numerically solving an initial value problem in which a wave packet propagates toward a critical level, where it breaks down into much smaller scale motions. The equations of motion for the (dimensionless) velocity vector $\vec{u}(\vec{x},t) = (u,v,w)$ and the perturbation density ρ, with respect to an ambient linear profile $\Theta(z)$, are listed below.

$$\frac{\partial \vec{u}}{\partial t} + \vec{u} \cdot \nabla \vec{u} = -\nabla p - Ri\rho\hat{z} + Re_*^{-1} \nabla^6 \vec{u} \tag{1a}$$

$$\frac{\partial \rho}{\partial t} + \vec{u} \cdot \nabla \rho - w = Pr_*^{-1} Re_*^{-1} \nabla^6 \rho \tag{1b}$$

$$\nabla \cdot \vec{u} = 0 \tag{1c}$$

The parameter Ri is the bulk Richardson number defined as $Ri = [NL/U]^2$ with constant $N^2 = -g/\rho_0 \, d\Theta/dz$. The equations are solved in the unit cube $0 \le x,y,z < 1$ with periodic boundary conditions in all space dimensions. The grid is uniform, with 32 points in each horizontal direction and 200 points in the vertical. A pseudo-spectral numerical algorithm, with second order Adams Bashforth time stepping is used to evolve the flow field in time.

Sub-grid scale model:

A sub-grid scale model is incorporated through the inclusion of "hyper" viscous and diffusive operators. Mathematically, the physical Laplacian operators and their coeffecients have been replaced with nonphysical ∇^6 operators and new coefficients. The magnitude of the coefficients

depends on the grid resolution. For high resolution grids, these parameters can be extremely small since the sixth order derivative introduces a factor of wavenumber to the sixth power. By choosing these coefficients to be small, $O(10^{-17})$, the viscous/diffusive effects can be confined to the narrow region of wavenumber space near the resolution limit. This leaves the remainder of wavenumber space to be treated essentially inviscidly and nondiffusively. To contrast, a second approach would be to leave the physical terms in the equations and choose an unphysically small Reynolds number. The form of sub-grid scale model chosen preserves the diffusive character of the small scale processes and is convenient to implement in a spectral scheme. It does, however, have important physical implications and needs some justification for the present study. We note that *any* diffusive mixing that occurs in the simulation will be done by "hyperdiffusion" and hence must be regarded as occurring at subgrid scale. In employing this form of sub-grid model, two important assumptions are made. First, we assume that the overall rate of dissipation and diffusion is controlled fundamentally by the rate of downscale energy transfer and not by the specific form of the viscous/diffusive operators. Second, we assume that the transfer of energy back upscale from the sub-grid scales is unimportant.

Initial conditions:

An ambient horizontal shear flow $U(z)$ and a downward propagating internal wave packet are specified as initial conditions. The wave packet is specified to be two-dimensional, with variations in the x and z directions only, with nondimensional wavelengths of 1 and 1/8 respectively. The packet is localized in the vertical by a slowly varying Gaussian envelope. The form of the ambient flow U is chosen so that a critical level is present at $z_c = 0.54$. A broad band spectrum of small amplitude, three-dimensional "noise" is also initialized, allowing the flow to evolve into three dimensions.

Flow evolution:

The equations are integrated forward in time for 50 buoyancy periods. The wave packet propagates downward from a region of no shear into the ambient flow. Refraction of the wave by the mean shear impedes its progress and reduces the intrinsic scale of the wave motion. The wave steepens near the critical level and creates regions of overturned isopycnals and strong shear before "breaking" into small scales which then dissipate and diffuse.

Figure 1 shows profiles of displacement taken at a fixed horizontal location at several points in time. The initial Eulerian phase speed of the wave packet is zero. The intrinsic right going phase propagation is balanced near the top of the figure by a left flowing mean current. The current speed is zero at z_c, where the wave becomes critically refracted. The prescribed wave envelope is nearly zero in the region shown in the figure, thus the displacements are initially small. Later, the wave has propagated into the region from above, resulting in finite displacements. Figure 2 shows contours of the density field sampled at the same horizontal location. Note the overturns in the isopycnals near the critical level at about t=20. Clearly, the most interesting flow dynamics occur in this "wave breaking" region. The remainder of the paper will concentrate on the diagnosis of the diffusive mixing associated with the flow in this region.

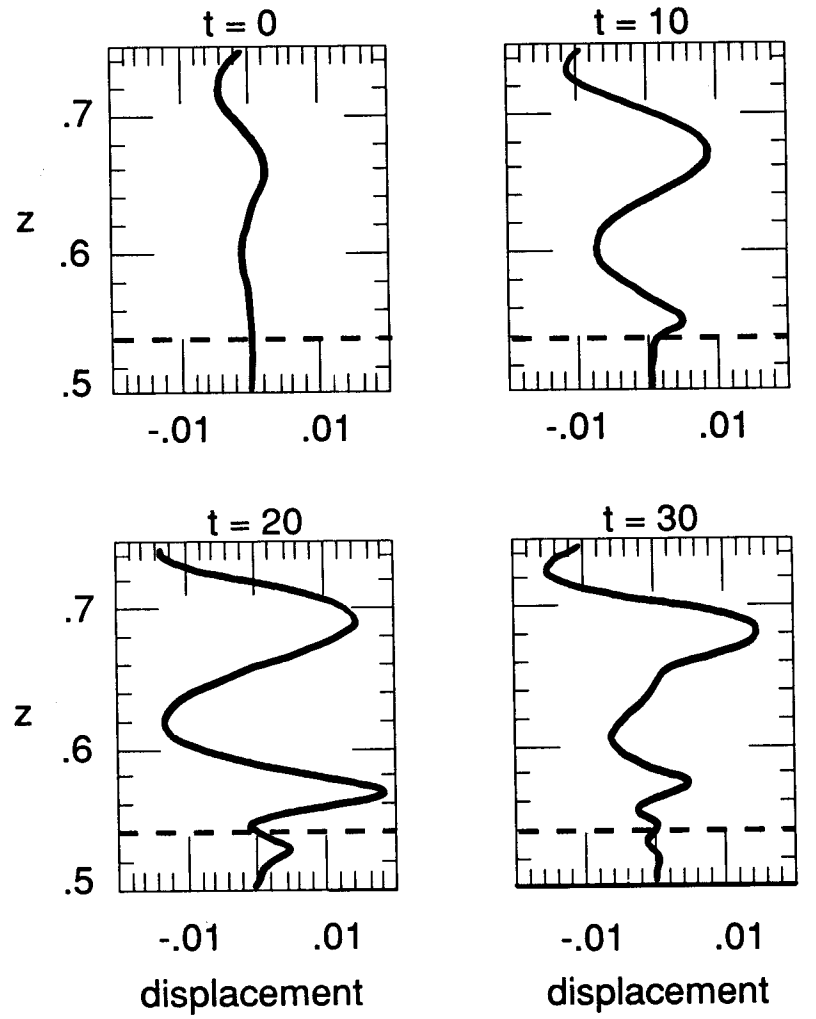

Figure 1. Vertical profiles of (dimensionless) isopycnal displacement are shown at several times t (in buoyancy periods). The wave packet propagates downward toward a critical level, depicted by the broken line.

DENSITY VARIANCE AS AN INDICATOR OF MIXING

We begin our discussion of mixing by looking at the dynamical balance of the density variance equation. The equation for the density perturbation from an ambient linear gradient is

$$\frac{\partial \rho}{\partial t} + \vec{u} \cdot \nabla \rho - w = D(\rho) \tag{2}$$

where $D(\rho)$ is simply the "hyperdiffusion" term appearing in Eq. (1b). The perturbation density ρ can be further decomposed into horizontal mean and fluctuating components; $\rho = \bar{\rho} + \rho'$. Multiplying Eq. (2) by the fluctuating component ρ' and horizontally averaging, denoted by an overbar,

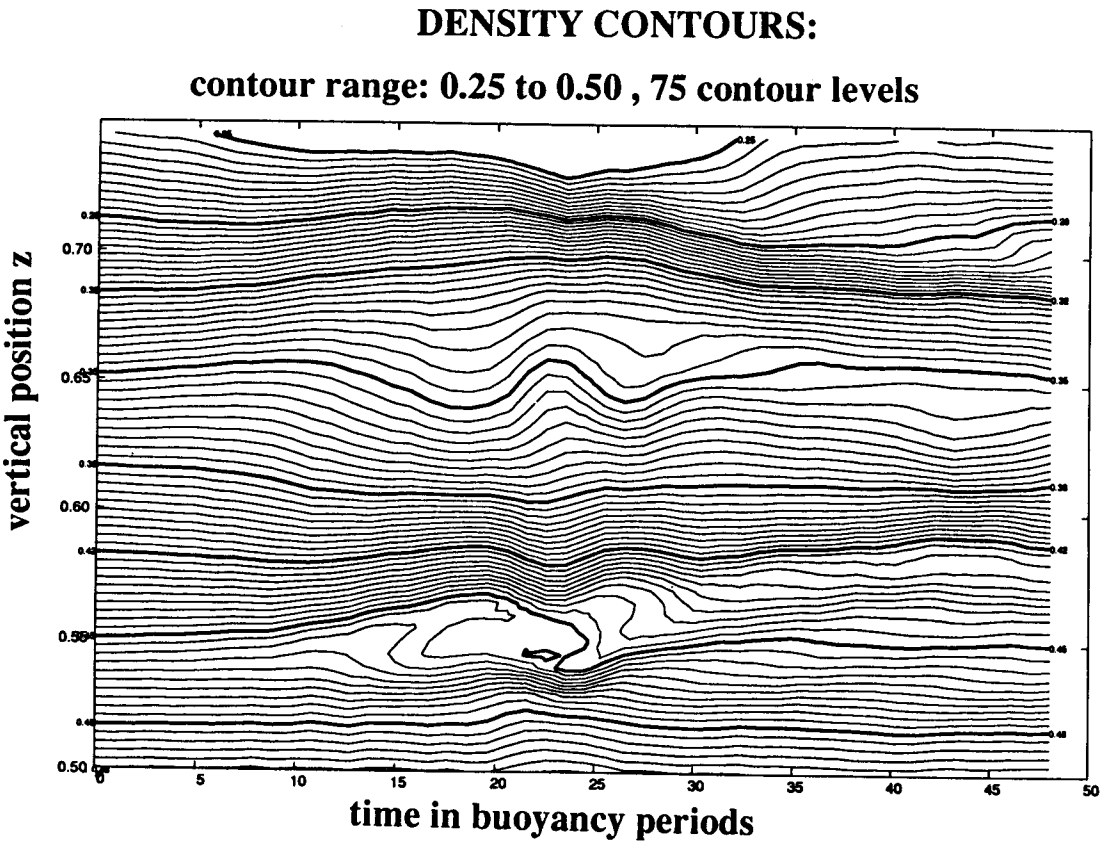

Figure 2. The density profiles obtained at a fixed horizontal location are contoured in the depth-time plane. Overturned isopycnals are apparent near $t = 20$ when the wave breaks.

gives an equation governing the production of density variance.

$$\frac{\partial}{\partial t}\overline{\rho'^2} = -\frac{\partial}{\partial z}\overline{\rho'^2 w} - 2\overline{\rho w}\frac{d\rho_{tot}}{dz} + \overline{\rho' D(\rho')} \qquad (3)$$

The horizontally periodic boundary conditions have been taken into account in the derivation of Eq. (3). The quantity ρ_{tot} is the horizontally averaged total density. The terms on the right hand side of this equation can be thought of as forcing terms, producing density variance. Eq. (3) states that density variance can be generated by advection across the vertical boundaries, buoyancy flux, or diffusion. Similar equations can be derived for temperature variance or "turbulent" kinetic energy. Indirect microstructure measurement techniques are based on approximate balances within these equations, which are assumed to be valid in the ocean interior when "ensemble averaged" over many profiles. Here we focus on the behavior of Eq. (3), integrated over the depth interval of interest, enclosing the critical level and the wave breaking region.

Figure 3 shows the volume integrated ρ'^2 as a function of time. Note that its production is strongly time dependent; there is no interval of time when Eq. (3) can be reasonably approxi-

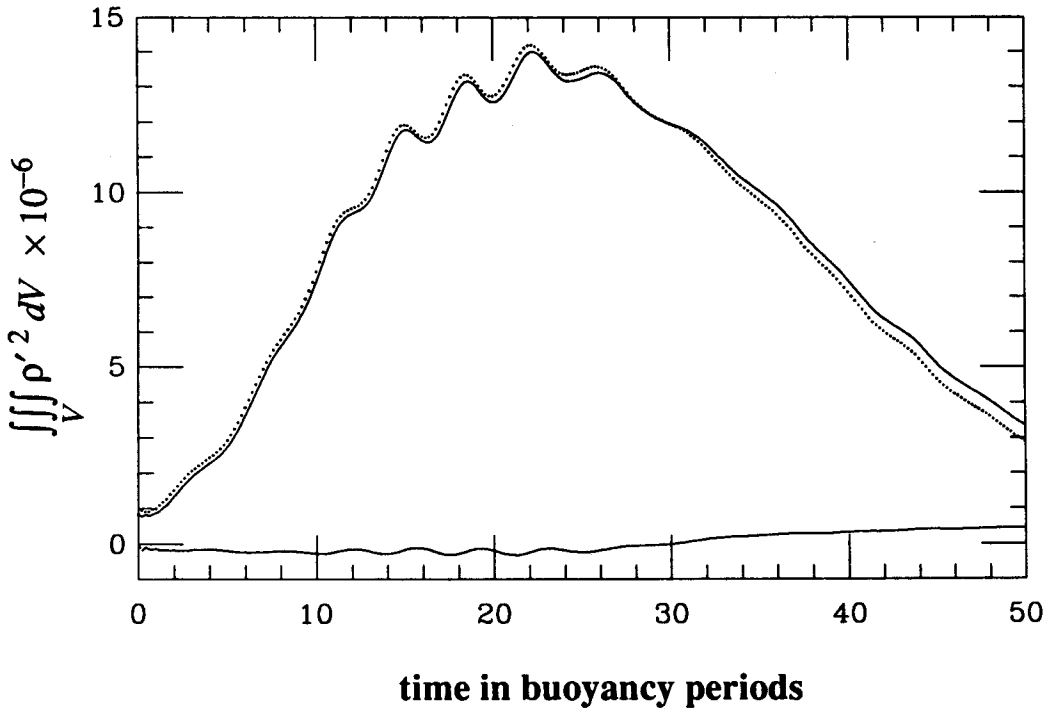

Figure 3. The upper solid curve is the volume integral of ρ'^2. The dotted curve was obtained by integrating the production terms on the right-hand side of Eq. (3) in time. The small residual between the two calculations is also shown.

mated as steady state. Note also that changes in density variance are not irreversible, density variance increases rapidly and then decreases just as efficiently, with a relatively small residual left behind when the calculation was terminated. Normally, when we think of mixing by an isolated turbulent event, we think of a nearly irreversible process, with a localized mixed layer perhaps eventually diffusing away, but only on very long time scales after the turbulence dies out. It seems reasonable to conclude that the production of density variance is influenced, or even dominated by, nonmixing processes. It is not clear how to use Eq. (3) to diagnose the mixing associated with this event.

The role of the buoyancy flux

Further insight can be obtained regarding the temporal behavior of Eq. (3) by looking at the role played by the buoyancy flux $\overline{\rho w}$. Figure 4a shows the vertically integrated buoyancy flux as a function of time. The buoyancy flux shows strongly oscillatory behavior on a short time scale approximately corresponding to the initial wave period. The magnitude of these oscillations can be quite large, even causing the signal to oscillate sign. It appears obvious that there is a strong wave component to the buoyancy flux. This is not too surprising, it would be reasonable to look at this signal temporally averaged to remove the intrinsic wave oscillations. The broken curve is a crude approximation of the time averaged signal. The averaged buoyancy flux is positive until about $t = 20$, when the wave breaks. It then changes sign and remains negative throughout the rest of the calculation.

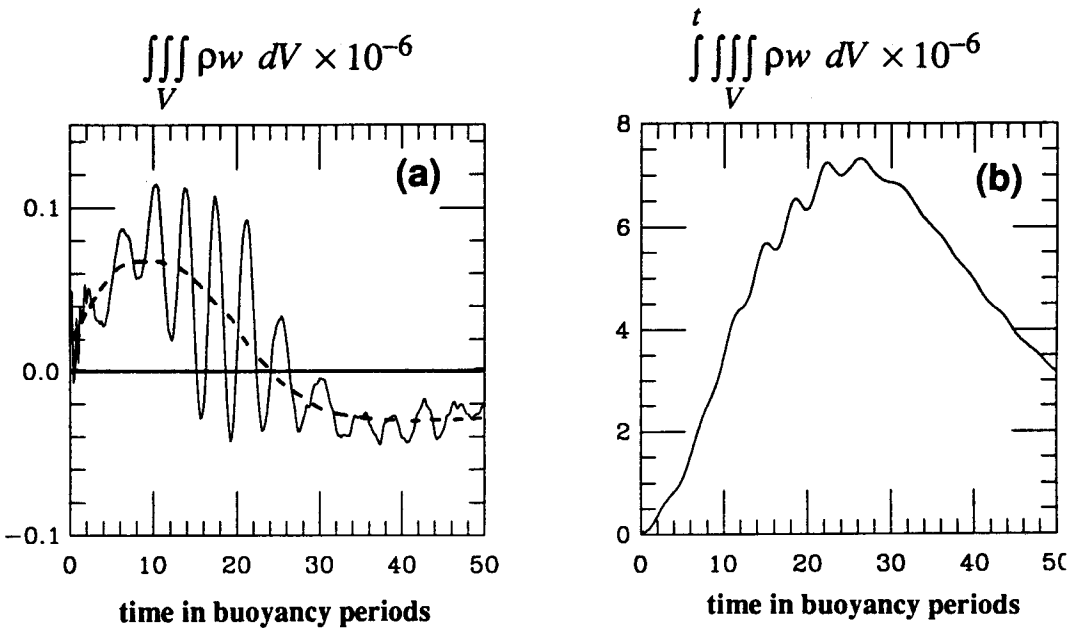

Figure 4. The volume integrated buoyancy flux is given by the solid curve in (a). The broken curve is an estimate of the time averaged signal removing the wave oscillations. The integral in time of the solid curve is given in (b).

Even the time averaged buoyancy flux is dominated by wave effects. As the wave approaches the critical level, the initially undisplaced density field is disturbed. Fluid parcels are displaced away from their equilibrium locations, resulting in a positive buoyancy flux. This process continues until about t=20, the time of wave "breaking". Two processes occur after the wave breaks. On the average, the displaced fluid parcels return towards their equilibrium positions, and some diffusion occurs at small scales as they do so. Parcels returning towards equilibrium give rise to a negative or counter-gradient buoyancy flux while diffusion results in mixing.

To illustrate the dominance of the wave effects on the density variance dynamics, we have integrated the net buoyancy flux of Figure 4a with respect to time and shown the result in Figure 4b. The similarity between Figures 3 and 4b implies that wave dynamics, through the buoyancy flux term, plays the dominant role in the density variance equation. For this event at least, using the density variance equation is not a particularly clean way to diagnose the mixing of the event. In essence, we conclude that spatial averaging does not adequately separate mixing from nonmixing processes. Loosely, we have not been able to separate "waves" from "turbulence".

DIRECT VIEW OF MIXING

We will now attempt to look at the mixing of the wave breaking event in a more direct manner. We will exploit a simple and intuitive concept, namely that diapycnal mixing results in changes in the volume of fluid found between a given pair of isopycnal surfaces. We can think of a stratified fluid at some time t_0 as a continuous distribution of isopycnal surfaces, along with an

associated velocity field. By discretizing the density range, we can think in terms of a finite number of these surfaces, each pair enclosing a finite volume of fluid. Suppose the fluid now evolves, undergoing both diabatic and adiabatic processes. At some later time t_1, the topology of these surfaces may be extremely complicated. To diagnose the amount of mixing, however, we are interested only in a single variable, the total volume of fluid between each pair. Figure 5a shows a schematic of the density field of a fluid that evolves from a state of uniform density gradient to a nonuniform, mixed state. Initially there is an equal volume in each of the density "bins". Later the volume in the middle bin has increased at the expense of the neighboring bins.

Obviously, the volume between the isopycnal surfaces has a functional dependence on the density field $\rho(\vec{x},t)$. This dependence, however, is very different than the usual horizontal or temporal averages we normally employ. Thinking of the total volume of fluid as a collection of fluid par-

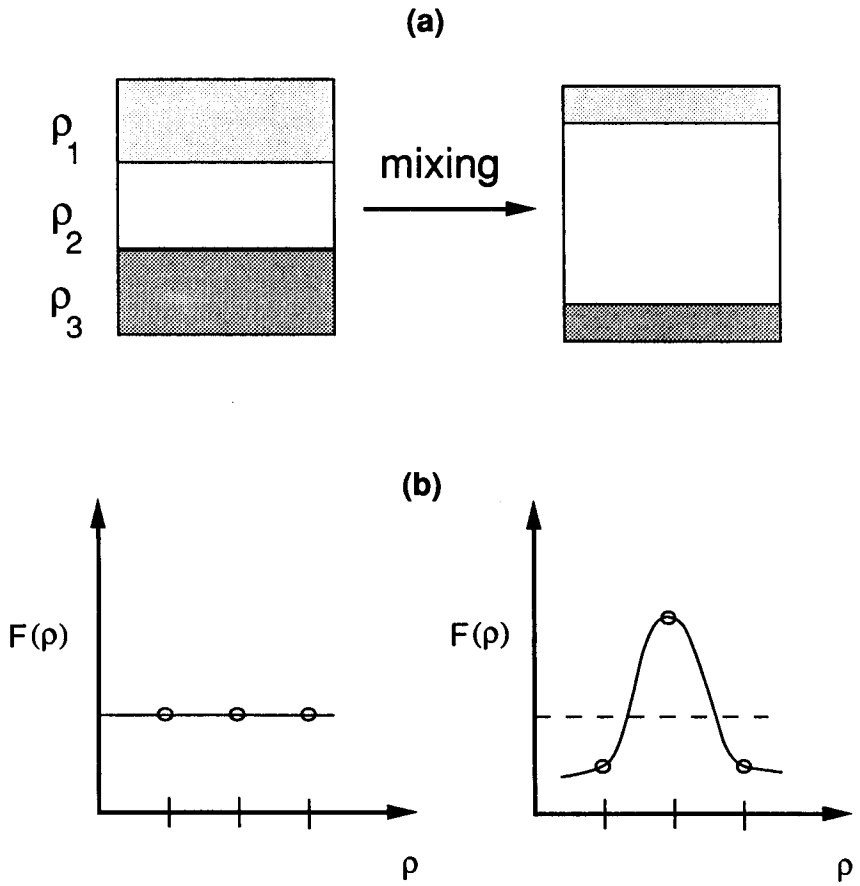

Figure 5. A schematic of a density stratified fluid is given in (a). The density range has been discretized into three "bins". Initially, the volume of fluid within each density bin is equal. After a mixing event, the volume of fluid in the central bin has increased while the volumes of the neighboring bins have decreased. Regarding the fluid as an ensemble of parcels, (b) shows the probability F of a randomly selected parcel having a density value within a given bin. Initially, the probabilities are equal. Later, the probability of finding a value within the central bin is greater. The function F depends on density but not on position.

cels, each with a density and velocity value, we can denote the probability of a randomly selected parcel having a density value of ρ as $F(\rho)$. Figure 5b shows the probability distribution F of the hypothetical density field of Figure 5a. Initially, there is an equal probability of occurrence for all values while later it is much more probable that a given parcel will have a value near ρ_2. The main difference between this type of functional dependence on density and, say, the horizontal average, is the lack of dependence on the vertical position of each parcel.

This simple idea can be incorporated into a straightforward algorithm for diagnosing mixing; at least in numerical simulations. For a given discretization of the density range, the volume of fluid can be computed directly for each pair of neighboring isopycnals. Each differential volume can be "spread out" over a constant area A, yielding a differential thickness for each "bin". The bins are then "stacked", with the densest fluid on the bottom at some fixed reference height, in order of decreasing density. By keeping track of the thickness of each bin, the locations of the edges of each bin are also determined. One can think of this algorithm as producing the "pseudo-positions" z_* of the given set of isopycnal values, *i.e.* a one-dimensional "sorted" density field which happens to be specified on an unevenly spaced grid.

Figure 6 shows contours of density in the (t, z_*) plane. In the absence of mixing, these contours would remain flat with a uniform vertical spacing. Deviations from flat isopycnals imply diapycnal mixing. The net spreading of isopycnals near $t = 20$ and $z_* = 0.54$ indicates the formation of a mixed layer. This mixed layer is bordered, both above and below, by regions of net isopycnal convergence where the background density gradient is enhanced. The lowest several isopycnals remain approximately flat, implying a lower level across which there is no mixing.

AVAILABLE AND BACKGROUND POTENTIAL ENERGY

These same ideas can be formulated in terms of energetics using the concepts of available and background potential energy. The concept of available potential energy has been discussed and applied by many authors including Lombard (1989), Dillon (1984) and Holliday and McIntyre (1981). The object is to define a one-dimensional "background" state for density that is insensitive to adiabatic dynamics and compute the potential energy associated with it. Changes in the background potential energy can then only occur through diffusive mixing. At some time t, the potential energy of a flow, in dimensionless form, is given by

$$E_p(t) = Ri \iiint_V \rho(\vec{x},t)(z - z_0)\, dV \tag{4a}$$

where z_0 is an arbitrary reference location.

Let z_* be the "pseudo-position" variable, defined by computing differential volumes, "sorting" and "stacking", in the limit as the isopycnal spacing goes to zero. The background potential energy E_b is simply the potential energy of the flow in pseudo-position space.

$$E_b(t) = Ri \iiint_V \rho(\vec{x},t)(z_* - z_0)\, dV \tag{4b}$$

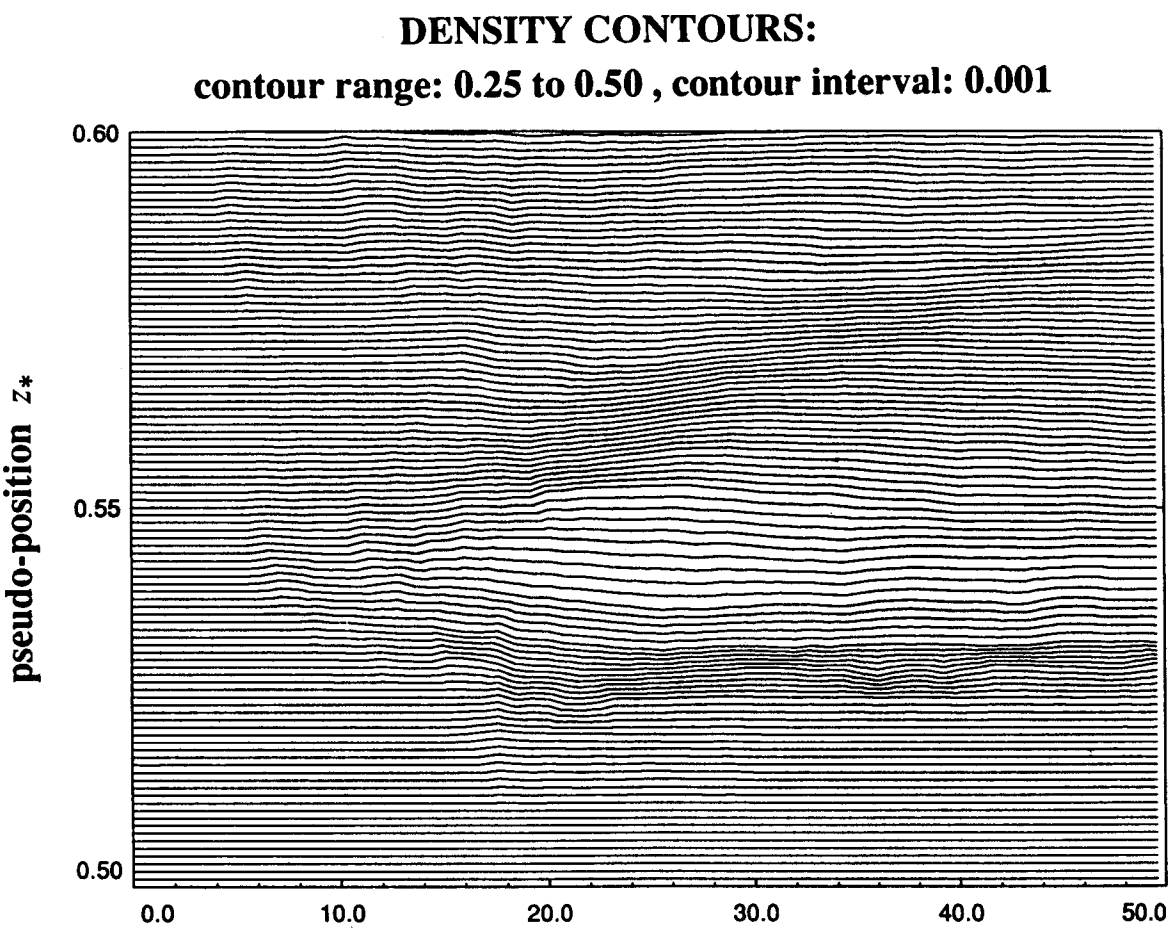

Figure 6. Contours of density in the (t, z_*) plane. Deviation from flat, regularly spaced contours indicates diapycnal mixing of the fluid. The main feature is the region of strong isopycnal spreading corresponding to the time and (true) position of the wave packet breaking near the critical level. Regions of net isopycnal convergence are also evident.

It is clear from this definition that the background potential energy is independent of true position z, depending only upon the ordered position z_*. For a given density value, z_* remains constant in time in the absence of mixing and can only change if mixing occurs.

The available potential energy E_a is defined as the total energy released by the flow in attaining the sorted state adiabatically.

$$E_a(t) = Ri \iiint_V \rho(\vec{x},t)(z - z_*)\, dV \qquad (4c)$$

Eqs. (4) define a unique decomposition of potential energy into available and background parts, *i.e.* $E_p = E_a + E_b$.

We denote the cumulative change in time of the background potential energy by $E_{mix} = E_b(t) - E_b(0)$. E_{mix} would seem to be a good indicator of diffusive mixing in a stratified fluid.

There are some subtleties, however. A volume must be specified over which the analysis will be applied. For the present discussion, we will work in an Eulerian reference frame and specify a fixed volume in space. It is instructive to take the time derivative of Eq. (4) to see how the potential energy in such a volume can change.

$$\frac{d}{dt} E_p = (z - z_0)\,\overline{\rho w}\,|_{z_2}^{z_1} + Ri \iiint_V \rho w \, dV + \iiint_V (z - z_0)\, D(\rho)\, dV \qquad (5)$$

We immediately encounter a difficulty. The first term on the right hand side of Eq. (5) indicates that the total potential energy changes as a result of net mass flux across the upper and lower boundaries. Although the volume remains constant in an Eulerian framework, the mass is not necessarily conserved within the volume. Care must be taken in interpreting a potential energy budget of an open system in which the mass is changing.

Note that this difficulty arises in this problem because we choose to apply our energetics analysis to only a small domain in which the wave breaking occurs. Had we used the entire computational domain, we would have had boundary conditions on the top and bottom to impose. For some boundary conditions, *i.e.* no slip wall conditions, the vertical velocity is zero, the mass flux terms are zero, and there is no problem. Spectral methods, however, are commonly used for simulating stratified turbulence and can create difficulties in analyzing potential energy even when the entire domain is used. Often, periodic boundary conditions are specified for velocity and *perturbation* density (from, say, a linear ambient profile) in all space directions. Such conditions are often interpreted loosely as "waves that propagate out through one boundary propagate back in through the paired boundary". Note, however, that this implies that parcels from near the bottom of the domain can be interchanged with parcels from near the top by wavelike oscillations. In other words, the total mass is not conserved and care must be used in quantifying the potential energy of the flow.

In general, the analysis could be performed in isopycnal coordinates. For a volume bounded by two isopycnals, across which no mixing occurs, both the volume and the mass remain constant. If two such bounding isopycnals can be found, the analysis can, in principle, be performed cleanly.

For our particular problem, however, we can compensate for the nonconservation of mass in one of two ways. The cumulative changes in potential energy due to net mass flux can be computed explicitly and the potential energy budget "corrected" for this effect. A second approach takes into account the fact that the mass flux occurs primarily at the top boundary. The lower boundary is located below the critical level, which prevents most of the wave energy from reaching it. The difficulty, then, is the net interchange of parcels near the top boundary but inside V, with parcels of slightly different density outside V. From Eq. (5) we see that the problem can be minimized by selecting the reference location z_0 to coincide with the top boundary z_2. Exchanging parcels with different densities at exactly this level then results in no change in potential energy

while exchanges of parcels near this value have only small effects. Either of these corrections are adequate for our purposes here. We have chosen the second technique for the energetics balance below.

Figure 7 shows the available and background potential energies as a function of time. The available potential energy behaves much like the net integrated buoyancy flux of Figure 4b. E_a increases prior to wave breaking as parcels are displaced on the average, and decreases after the wave breaks, as parcels return towards their equilibrium values. The background potential energy, however, behaves quite differently. Prior to wave breaking, it remains approximately constant as the flow contains no appreciable energy at the diffusive scales. After wave breaking, the fluid mixes as small scale features diffuse while returning towards equilibrium.

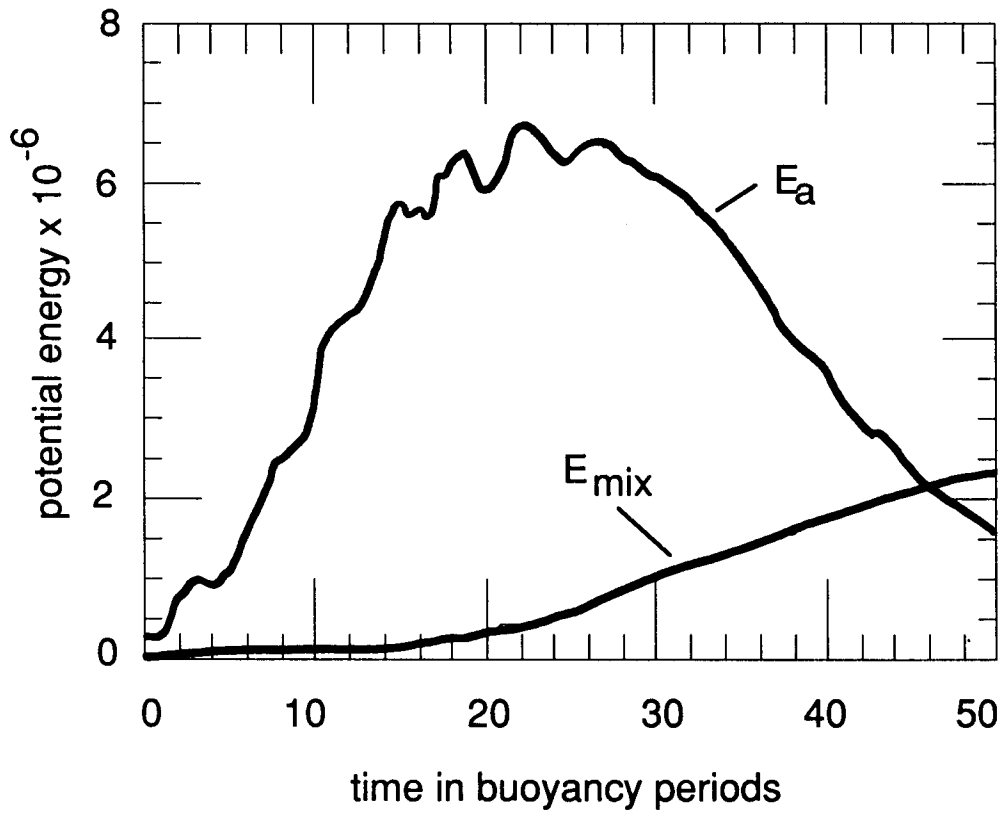

Figure 7. The available potential energy E_a and the cumulative change to the background potential energy E_{mix} are shown as functions of time. E_a increases initially as the packet propagates into the volume and displaces the stratification and decreases after wave breaking as parcels return towards their equilibrium positions. The increase in E_{mix} at later times indicates that diffusive mixing takes place as the fluid restratifies.

VERTICAL DIFFUSIVITY K_d

The function $\rho(t,z_*)$ is an interesting and useful quantity. We can think of it as "mean" density field where the averaging operator filters out small-scale details of the flow, like the displacements of fluid parcels due to internal wave motion, but retains the overall effects of small-scale mixing. It is this sort of averaging that is implicit in the formulation of meso to large-scale circulation models. In such models, internal waves and turbulence occur at scales much too small to resolve, but the overall mixing accomplished by these motions must be incorporated in some manner.

Earlier, we interpreted the spreading and convergence of the isopycnals in Figure 6 as a qualitative indicator of diffusive mixing. We can also use $\rho(t, z_*)$ in a more quantitative manner by computing the rate of spreading. Suppose we introduce a model evolution equation for the "mean" density field.

$$\frac{\partial}{\partial t}\rho(t,z_*) = \frac{\partial}{\partial z_*}Q(t,z_*) = \frac{\partial}{\partial z_*}K_d\frac{\partial \rho}{\partial z_*} \tag{6}$$

Although the mean state changes as a result of complicated three-dimensional motions at small scales, Eq. (6) collapses the net effect onto a single vertical diffusivity function K_d . K_d can be computed directly from the mean density field and the overall character of the mixing event can be examined with respect to pseudo-position z_* and time.

$$K_d(t,z_*) = \frac{\int^{z_*}\frac{\partial \rho}{\partial t}(t, z_*')\,dz_*'}{\frac{\partial \rho}{\partial z_*}} \tag{7}$$

Figure 8 shows contours of the (dimensionless) diffusivity function K_d. The main feature in the figure is located near $z_* = 0.54$ and $t = 20$, which corresponds to the time and place that the strongest wave breaking occurred. The diffusivity is positive in this region, corresponding to local spreading of isopycnals. This feature is responsible for most of the mixing of the event. It is relatively brief in duration, lasting only about 5 buoyancy periods. After the main mixing event, the diffusivity field becomes much more complicated, with both positive and negative features appearing. The negative values correspond with the regions of converging isopycnals in Figure 6. Figure 9 shows the result of time averaging the diffusivity field.

MIXING EFFICIENCY

We define the mixing efficiency of the event γ_{mix} as follows.

$$\gamma_{mix} = \frac{\text{rate of increase of background potential energy}}{\text{rate of dissipation of kinetic energy}} \tag{8}$$

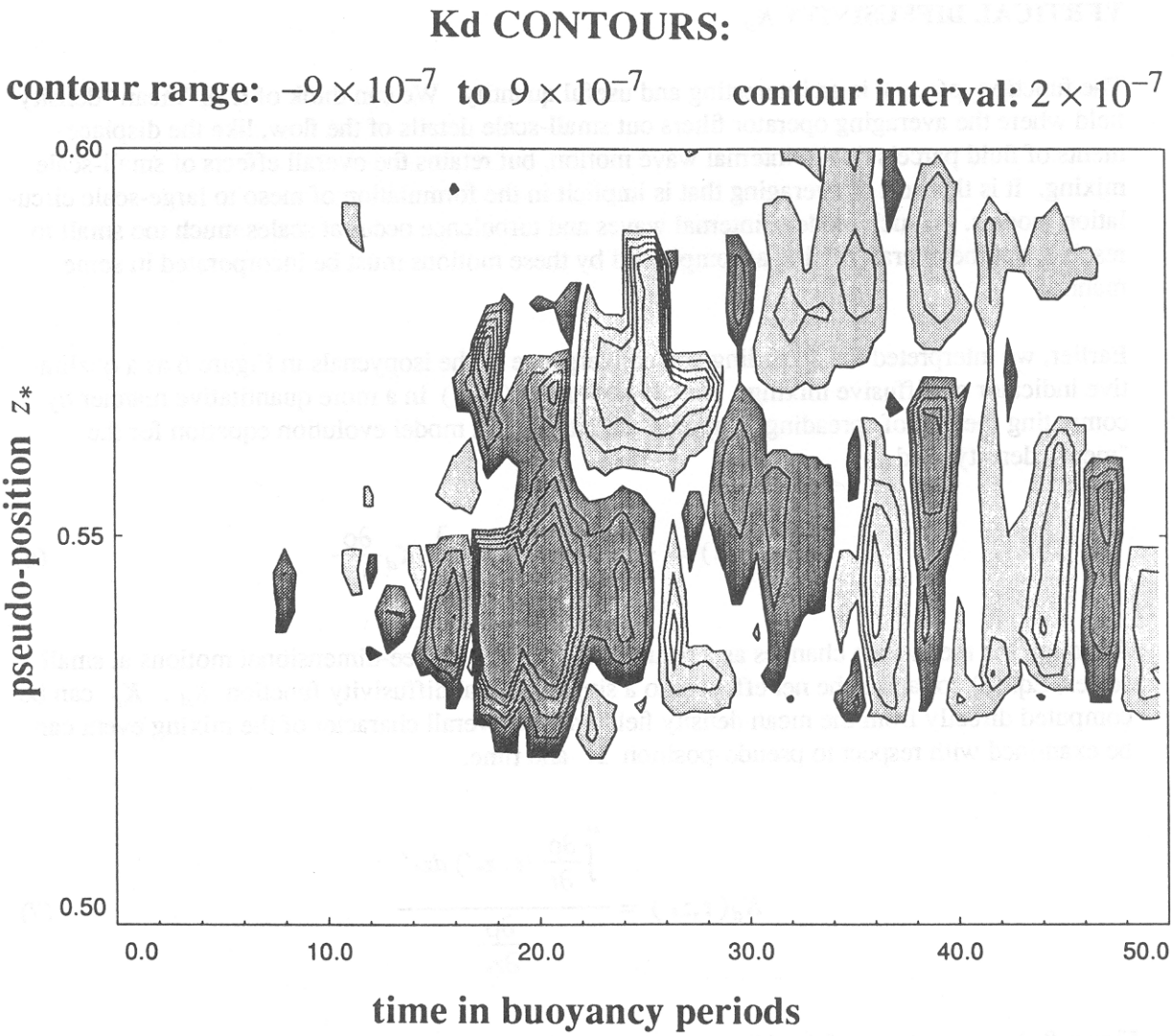

Figure 8. Contours of the vertical diffusivity of mass K_d defined in Eq. (7). A strong positive feature is seen to correspond with the initial region of wave breaking. At later times, the field becomes more complicated with both positive and negative diffusivities appearing.

The rate of increase of background potential energy can be obtained by estimating the nearly constant slope from Figure 7. The dissipation rate of kinetic energy, ε is shown in Figure 10 along with the rate of dissipation of density variance χ. Taking a representative value of ε over the time period between $t = 20$ and $t = 50$, allows the ratio in Eq. (8) to be computed, yielding

$$\gamma_{mix} \approx 0.38 . \qquad (9)$$

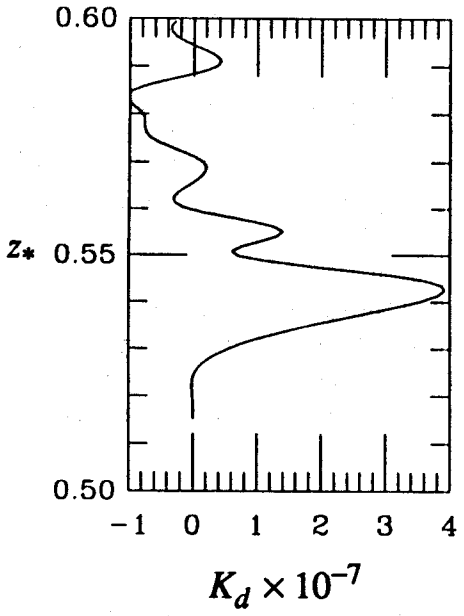

Figure 9. The time averaged profile of the diffusivity K_d.

Perhaps not surprisingly, approximately the same value is obtained if the mixing efficiency is defined as the ratio of representative values of χ to ε. We are encouraged that direct simulations can produce mixing efficiencies near the expected value, but more study is required to determine the sensitivity of this result to changes in the sub-grid scale model.

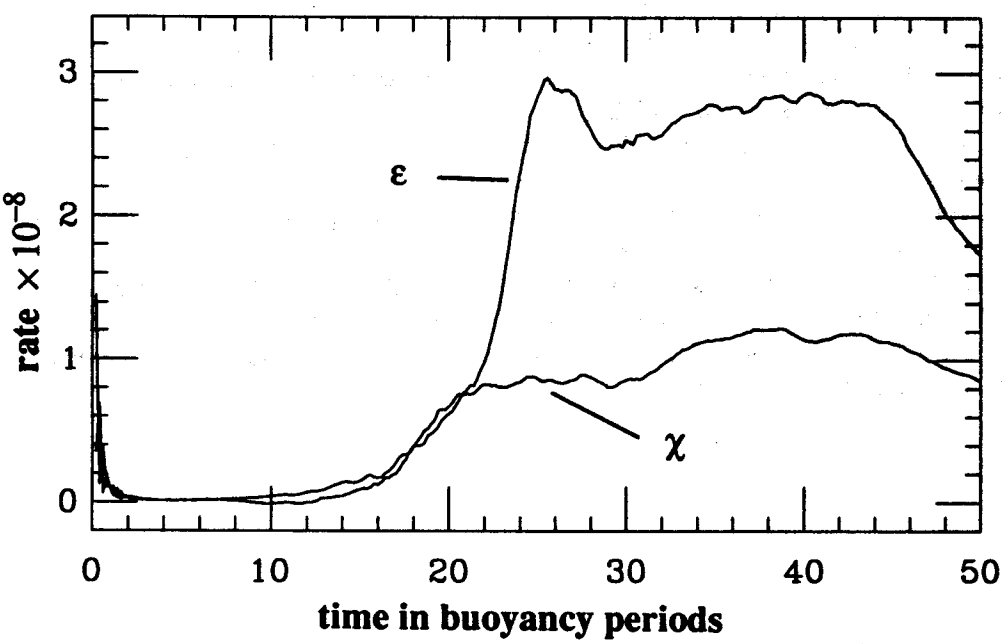

Figure 10. The dissipation rates of kinetic energy ε and density variance χ.

SUMMARY

We have examined the diapycnal mixing associated with a numerically simulated mixing event similar to what may be seen in the ocean interior. A high resolution, three-dimensional primitive equation model was used to simulate a wave packet breaking at a critical level. The temporal behavior of the density variance equation was discussed in relation to the diagnosis of the mixing of the event. The wave component of the buoyancy flux was shown to dominate the dynamics, obscuring the diagnosis. A direct approach, based on the computation of fluid volume between discrete isopycnal surfaces, was shown to be a less ambiguous indicator of the mixing dynamics. The results of this calculation were used to estimate the vertical diffusivity of mass K_d. Coupling this analysis with an energetics budget based available and background components of potential energy, a reasonably complete picture of the mixing dynamics emerges.

ACKNOWLEDGMENTS

This work was supported by the National Science Foundation, grant OCE 8700108. Funds to attend the Hawaiian Winter Workshop were provided by the Applied Physics Laboratory at the University of Washington.

REFERENCES:

Dillon, T.M., 1984: The energetics of overturning structures: implications for the theory of fossil turbulence. *J. Phys. Ocean. 14*, 541-549.

Gregg, M. C., 1987: Turbulence in stratified fluids: A review. *J. Geophys. Res.* **92,** 5249-5286.

Holliday, D. and M. E. McIntyre, 1981: On potential energy density in an incompressible stratified fluid. *J. Fluid Mech.* **107,** 221-225.

Lombard, P. N., 1989: Energetics of a stably stratified turbulent flow. *Masters Thesis, University of Washington* 157 pp.

Moum, J. N., 1989: Measuring turbulent fluxes in the ocean - The quest for K_ρ. *Proceedings of the 1989 Hawaiian Winter Workshop* 145-156.

Winters, K. B. and E. A. D'Asaro, 1989: Two-dimensional instability of finite amplitude internal gravity wave packets near a critical level, *J. of Geophys. Res.*, **94:C9,** 12,709-12,719.

Winters, K. B. and J. J. Riley, 1991: Instability of internal waves at critical levels, *Dynamics of Atmospheres and Oceans* (in press).